TECHNICAL TRANSACTIONS | CZASOPISMO TECHNICZNE
MECHANICS | MECHANIKA
1-M/2016

MARKUS KOLANO, MANUEL BREHMER, MATTHIAS KRAUME*

NUMERICAL SIMULATION OF VISCOELASTIC FLUID FLOW IN STIRRED VESSELS

SYMULACJA NUMERYCZNA PRZEPŁYWU PŁYNÓW LEPKOSPRĘŻYSTYCH W MIESZALNIKU

Abstract

In this work, a tool for calculating viscoelastic flows with rotating geometries in OpenFOAM based on the finite-volume method is presented. The tool combines the split-stress tensor approach and viscoelastic differential constitutive equations with the sliding-mesh technique. With this tool, a CFD simulation was run for a geometry of a spherical stirrer in an aqueous solution of carboxyl cellulose. Additionally, a rheological characterisation of that solution was conducted. For validation, the simulations were compared with flow field data acquired through particle image velocimetry measurements.

Keywords: viscoelasticity, White-Metzner, PIV, OpenFOAM, dynamic mesh

Streszczenie

W pracy przedstawiono program OpenFOAM do wyznaczania przepływów płynów lepkosprężystych przy użyciu metody objętości skończonych. Program łączy założenia dla tensora naprężeń dzielonych z konstytutywnymi równaniami różniczkowymi płynów lepkosprężystych oraz techniką przesuwnych oczek siatki. Symulacje CFD przeprowadzono w mieszalniku wodnego roztworu celulozy karboksylowej, badano również charakterystykę reologiczną roztworu. W celu weryfikacji symulacje zostały porównane z wartościami przepływu w mieszalniku uzyskanymi metodą PIV.

Słowa kluczowe: lepkosprężystość, model White-Metzner'a, PIV, OpenFOAM, dynamiczna siatka

DOI:

* MSc. Eng. Markus Kolano, MSc. Eng. Manuel Brehmer, Prof. PhD. DSc. Eng. Matthias Kraume, Chair of Chemical & Process Engineering, Faculty of Process Sciences, Technical University of Berlin.

1. Introduction

Most of the fluids encountered in the chemical, food or cosmetic industries exhibit non-Newtonian flow behaviour. Viscoelastic effects can occur, altering flow patterns and dynamics in comparison to Newtonian fluids, especially when dealing with polymeric and biological fluids. In stirred tanks, these effects can lead to cavern formation and inversion of flow fields around impellers i.e., influencing mixing times, power input, shear stress, etc. For process design, the ability to quantify and predict these effects numerically is therefore of high interest in order to be able to choose optimal stirrer and tank geometries and process conditions.

In general, viscoelastic fluids can be viewed as a combination of a viscous and an elastic material. In contrast to Newtonian fluids, time-dependent stress relaxation is observed. When subjected to shearing, viscoelastic fluids develop normal stress differences, leading to phenomena like the Weissenberg effect [1]. Furthermore, stretching of these fluids causes elastic forces. Additionally, the viscosity dependence on shear rate is commonly non-linear.

For a rotating sphere stirring a viscoelastic fluid in a vessel, Ide et al. [2] found out that dependently of the viscoelasticity of the continuous phase, the general direction of the secondary flow field is changed: for polystyrene-styrene solutions with low concentrations (up to 20wt-%), both the primary and the secondary flow field are qualitatively similar to those of a Newtonian fluid; for higher concentrations (50wt-% or more), the fluid flows inwardly at the poles of the sphere and is expelled at the equator. Similar phenomena were found for a disc and a flat turbine.

Numerical simulations of these effects have already been conducted for a sphere with the finite element method, i.e. [3], but a tool to simulate viscoelastic flows for rotating geometries with a finite-volume method in non-commercial CFD software hasn't yet been developed. In this work, a tool capable of calculating viscoelastic fluid flow for complex rotating geometries is presented. For validation, a CFD simulation for a rotating sphere in an aqueous carboxymetyhl cellulose solution was compared to particle image velocimetry measurements. For the simulation, a rheological characterisation of the used solution was also conducted.

2. Materials and Methods

2.1. Mathematical Model

To calculate isothermal incompressible flows of viscoelastic fluids, the equations for mass conservation:

$$\nabla \cdot (u) = 0 \tag{1}$$

and momentum conservation:

$$\frac{\partial(\rho u)}{\partial t} + \nabla \cdot (\rho u u) = -\nabla(p) + \nabla \cdot \tau \tag{2}$$

have to be solved, with ρ denoting the density of the fluid, p the pressure, u the velocity vector and τ the stress tensor.

By splitting the stress tensor into a Newtonian solvent contribution τ_s and an polymeric contribution τ_p, both the influence of the solvent and the polymeric liquid can be taken into account:

$$\tau = \tau_s + \tau_p \tag{3}$$

with τ_s being defined by:

$$\tau_s = 2\eta_s D \tag{4}$$

where η_s is the dynamic solvent viscosity and D is the deformations rate tensor:

$$D = \frac{1}{2}\left(\nabla u + [\nabla u]^T\right) \tag{5}$$

In literature, numerous constitutive models have been developed to describe viscoelastic flow behaviour with a polymeric contribution to the stress tensor [4]. In this work, the differential White-Metzner model [5] is used:

$$\tau_p + \lambda_p(\dot{\gamma})\overset{\nabla}{\tau}_p = 2\eta_p(\dot{\gamma})D \tag{6}$$

with η_p being the polymeric dynamic viscosity, λ_p the relaxation modulus and the shear rate $\dot{\gamma}$ being defined by:

$$\dot{\gamma} = \sqrt{2D:D} \tag{7}$$

In Equation (6), $\overset{\nabla}{\tau}_p$ denotes the upper convected derivative of the stress tensor:

$$\overset{\nabla}{\tau}_p = \frac{D}{Dt}\tau_p - [\nabla u^T \cdot \tau_p] - [\tau_p \cdot \nabla u] \tag{8}$$

where $\frac{D}{Dt}$ is the material derivative:

$$\frac{D}{Dt}\tau_p = \frac{\partial}{\partial t}\tau_p + u \cdot \nabla \tau_p \tag{9}$$

Both the shear rate dependence of the relaxation modulus and the viscosity can be modelled by a Cross correlation:

$$\eta_P(\dot{\gamma}) = \frac{\eta_{P,0}}{1 + (k\dot{\gamma})^{1-m}} \tag{10}$$

$$\lambda_P(\dot{\gamma}) = \frac{\lambda_{P,0}}{1+(L\dot{\gamma})^{1-n}} \tag{11}$$

where $\eta_{P,0}$ and $\lambda_{P,0}$ are the constant dynamic viscosity and relaxation modulus at a zero shear rate respectively; *k*, *m*, *L* and *n* are adjustable parameters. Instead of a model, Carreau-Yasuda-models can also be used:

$$\eta_P(\dot{\gamma}) = \eta_{P,0}\left[1+(k\dot{\gamma})^a\right]^{\frac{m-1}{a}} \tag{12}$$

$$\lambda_P(\dot{\gamma}) = \lambda_{P,0}\left[1+(L\dot{\gamma})^b\right]^{\frac{n-1}{b}} \tag{13}$$

To take into account a constant dynamic viscosity $\eta_{P,\infty}$ and relaxations modulus $\lambda_{P,\infty}$ at high shear rates, a variation of the Carrau-Yassuda equation can be used:

$$\eta_P(\dot{\gamma}) = \eta_{P,\infty} + (\eta_{P,0} - \eta_{P,\infty})\left[1+(k\dot{\gamma})^a\right]^{\frac{m-1}{a}} \tag{14}$$

$$\lambda_P(\dot{\gamma}) = \lambda_{P,\infty} + (\lambda_{P,0} - \lambda_{P,\infty})\left[1+(L\dot{\gamma})^b\right]^{\frac{n-1}{b}} \tag{15}$$

With *a* and *b* being additional adjustable parameters.

2.2. Model Implementation in OpenFOAM®

In 2010, Favero et al [6] developed a volume of fluid tool to calculate transient, incompressible viscoelastic flows. They implemented numerous differential viscoelastic constitutive equations and released them in the OpenFOAM® Extend Project. Additionally, dynamic mesh handling is a supported feature in OpenFOAM® [7], allowing for both dynamic mesh movement as well as refinement.

The tool presented in this work combines the aforementioned features to calculate viscoelastic flows for rotating geometries. For velocity-pressure-stress coupling, a so-called PIMPLE algorithm is used, a method that results from combining the SIMPLE [8] and PISO [9] algorithms. The procedure used in the tool to solve the problem of viscoelastic fluid flow for rotating geometries can be summarised as follows:

1. As a first step, the initial mesh is altered according to the predefined mesh motion, updating boundary conditions, calculating relative fluxes with the given fields of velocity *u*, pressure *p* and stress tensor τ and interpolating them at arbitrary mesh interfaces.
2. Subsequently, the PIMPLE algorithm starts: the pressure gradient and the stress divergence are calculated explicitly and the momentum equation is solved implicitly for each velocity component.
3. With the new velocity field estimate, the pressure equation is solved and corrected.
4. If desired, an inner PISO corrector loop can be started, which repeatedly solves and corrects the pressure equation to obtain more accurate pressure and velocity fields.
5. Finally, the stress tensor field is calculated according to equation (6).
6. Steps 2, 3, 4 and 5 can be repeated as many times as desired before the PIMPLE-loop for the next time step starts at step 1 again.

2.3. Computational Grid and Solver Parameters

For the CFD simulations, the computational grid was created with the snappyHexMesh utility – an OpenFOAM meshing tool capable of refining the mesh at specific surfaces, feature lines and within certain cell. The dimensions of the grid were 0.3 m in all directions, with a sphere of 0.04 m diameter being in the centre of the mesh. The rotating region of the mesh was a cylindrical region with a diameter of 0.2 m and a length of 0.2 m, with the front and back side of cylinder being oriented normal to the x-axis, which was also the axis of rotation. The overall number of cells was 71,540, with 67,080 of them being hexahedra, 24 prisms and 4,436 polyhedra. The arbitrary mesh interface consisted of 21,053 faces, while the dynamic mesh region contained 67,538 cells. Convergence criteria for the velocity, pressure and stress tensor fields were a residual of $4\ 10^{-7}$ with a relative tolerance of 0, respectively. The time-step size was adjusted dynamically to a maximum Courant number of 1.

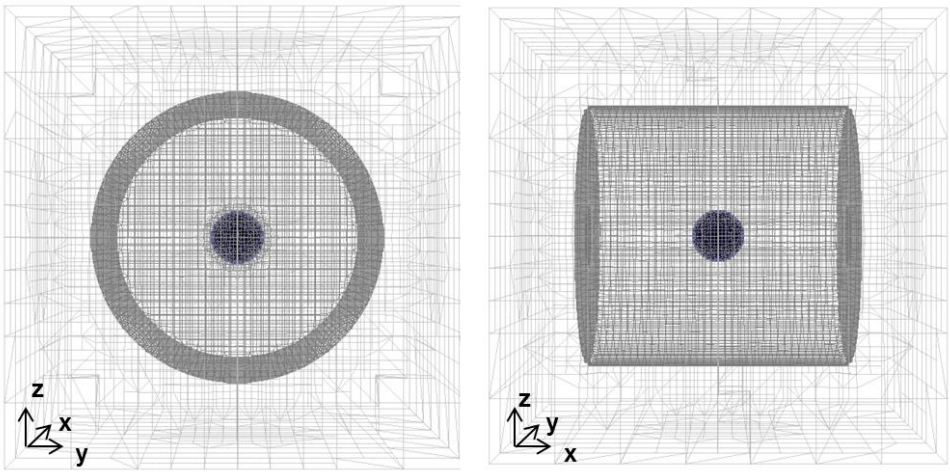

Fig. 2. Computational domain: surface mesh of sphere in black, dynamic mesh part in dark grey

2.4. Experimental Setup

For the experimental determination of velocity fields using the PIV-technique, a rectangular vessel was used. Length, height and width were 1m, 0.5 m and 0.5 m respectively. The material of the vessel walls was glass with a width of 0.01 m, allowing a laser light to pass through with a minimum of absorption and reflection from the vessel walls. As a stirrer, a stainless steel sphere with a diameter of 0.04 m was used. The sphere was connected to a horizontal shaft and was driven by a motor at a stirring speed of 1000 rpm and positioned in a central position 0.25 m away from the fluid surface and the vessel walls, except for the wall where the shaft was put through (0.15 m distance).

A LaVision FlowMaster 2D-PIV system was used for the PIV measurements in this study. It consisted of a pulsed Nd:YAG laser with a maximum double pulse rate of 15 Hz and the progressive-scan Imager Pro SX 5M CCD camera with a 12 bit range and a maximum resolution of 2456 by 2058 pixels. PIV-calculations were performed with the DaVis 8 software. To prevent damage to the camera due to uncontrolled reflections, fluorescent tracer particles in combination with a cut-off filter lens were used.

The laser was positioned at the same height as the stirrer on the opposite site of the motor, illuminating the symmetry plane normal to the vessel floor. Images were taken with a frame rate of five double images per second.

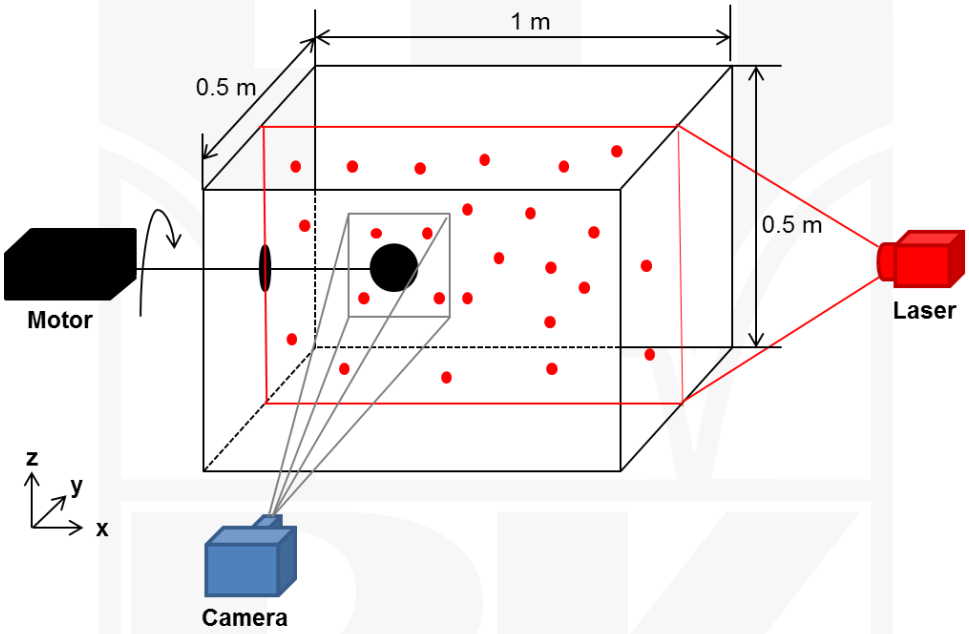

Fig. 2. Experimental setup for PIV measurements; the laser illuminates the symmetry x-z plane

2.4. Model Liquids and rheological characterisation

An aqueous carboxymethyl cellulose (Blanose) solution with a concentration of 5 g kg^{-1} was used as a viscoelastic model liquid. At higher concentrations, these solutions can become too opaque to allow for optical flow field measurements via the PIV method. Rheological measurements were carried out at 20°C with an Anton Paar MCR302 device, using a cone-and-plate system.

3. Results

3.1. Dynamic Viscosity and 1. Normal Stress Difference

In Figure 3, the results for the rheological measurement of the dynamic viscosity of the 5-wt% CMC solution as well as corresponding fits are presented. At shear rates lower than 0.06 s^{-1}, the accuracy of the used rheometer is not high enough to allow for exact measurements.

In general, the 5-wt% CMC solution exhibits shear thinning behaviour with a constant dynamic viscosity at low shear rates (about 0.22 Pas). With all aforementioned models, it is possible to acquire satisfactory fits, with the Carreau-Yasuda type models being capable of predicting the slope of the viscosity curve most accurately.

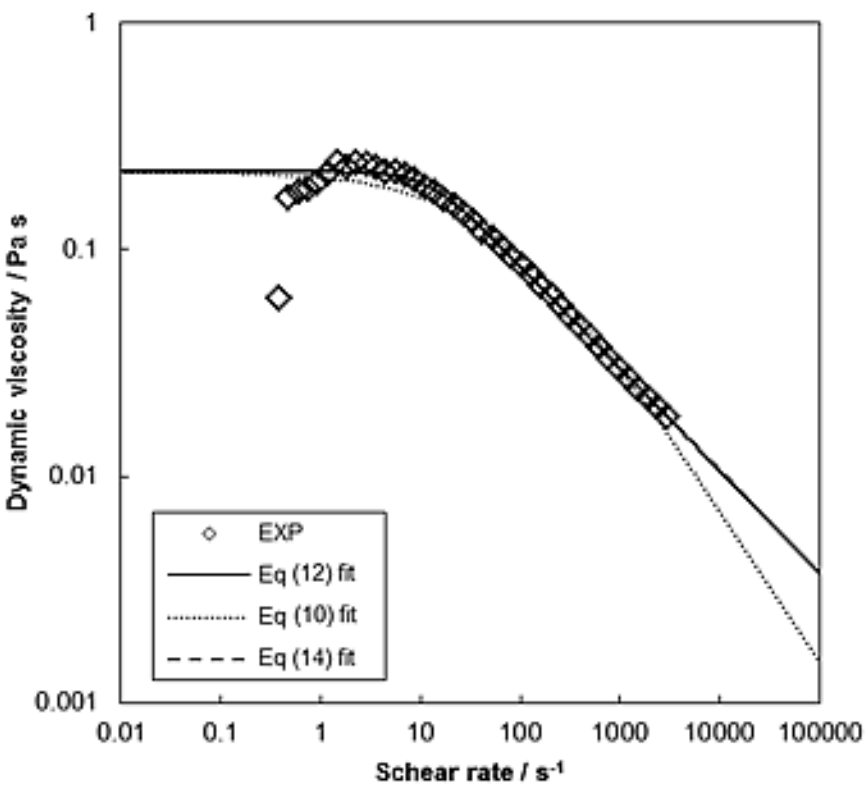

Fig. 3. Measured dynamic viscosity curve for 5-wt% CMC and corresponding fits

In Figure 4, the measured 1. normal stress differences for the same solution are shown. With increasing shear rate, the 1. normal stress differences rise. It has to be noted that measuring normal stress differences at low shear rates with the used rheometer is difficult

or impossible, since the measurement accuracy is too low to resolve the normal forces occurring under those conditions. The relaxation moduli were calculated from the dynamic viscosity and the 1. normal stress difference:

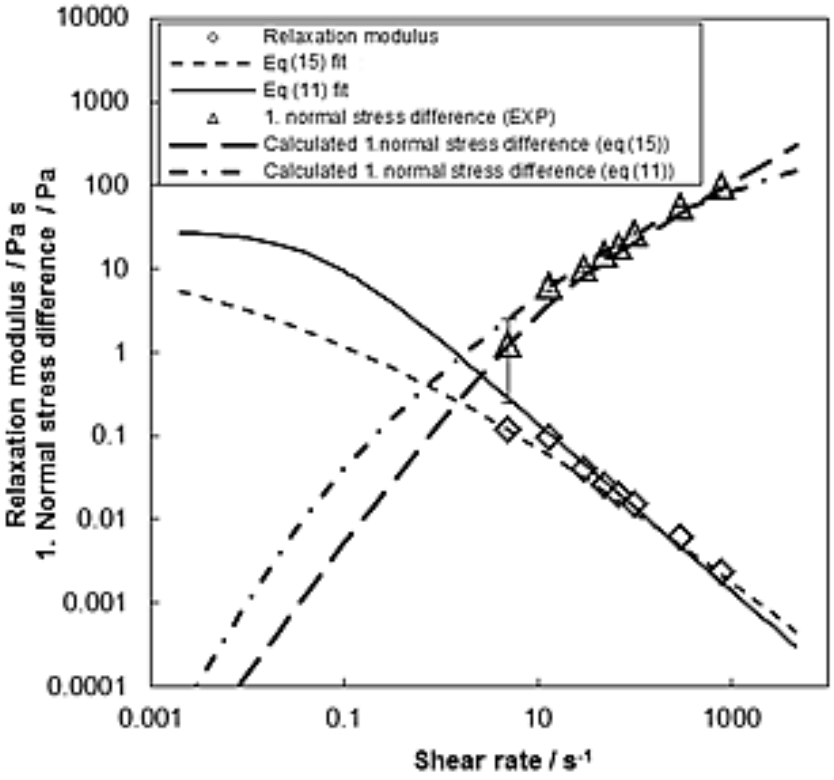

Fig. 4. Measured 1. normal stress differences for 5-wt% CMC and corresponding fits for relaxation moduli

Equations (11) and (15) were used to model the dependence of the relaxation modulus on shear rate, as shown in Figure 4. The best fit was achieved for the Carreau-Yasuda type model (Equation [15]).

$$\lambda_P = \frac{N_1(\dot{\gamma})}{2\eta_P(\dot{\gamma})\dot{\gamma}^2} \tag{16}$$

Finally, the model parameters for the fits in Figures. 3 and 4 are presented in Tables 1 and 2.

Table 1

Model parameters for the different viscosity models

	$\eta_{P,\infty}$ Pa s	$\eta_{P,0}$ Pa s	k s	m	a
$\eta_P(\dot{\gamma}) = \frac{\eta_{P,0}}{1+(k\dot{\gamma})^{1-m}}$	–	0.220	0.016	0.331	–
$\eta_P(\dot{\gamma}) = \eta_{P,0}\left[1+(k\dot{\gamma})^a\right]^{\frac{m-1}{a}}$	–	0.220	0.085	0.550	2.209
$\eta_P(\dot{\gamma}) = \eta_{P,\infty} + (\eta_{P,0} - \eta_{P,\infty})\left[1+(k\dot{\gamma})^a\right]^{\frac{m-1}{a}}$	10^{-5}	0.220	0.085	0.550	2.210

Table 2

Model parameters for the different relaxations modulus models

	$\lambda_{P,\infty}$ Pa s	$\lambda_{P,0}$ Pa s	L s	n	b
$\lambda_P(\dot{\gamma}) = \frac{\lambda_{P,0}}{1+(L\dot{\gamma})^{1-n}}$	–	28	20	0.001	–
$\lambda_P(\dot{\gamma}) = \lambda_{P,\infty} + (\lambda_{P,0} - \lambda_{P,\infty})\left[1+(L\dot{\gamma})^b\right]^{\frac{n-1}{b}}$	10^{-5}	28	8.637	0.002	0.213

3.2. Simulation Results

In Figures 5 and 6, velocity profiles for both the PIV measurements and CFD simulations are presented. In Figure 5, the velocities along the line through the origin and parallel to the *x*-axis are shown, while in Figure 6, the line is parallel to the z-axis. The transient simulation was stopped after a simulated time of 6 seconds.

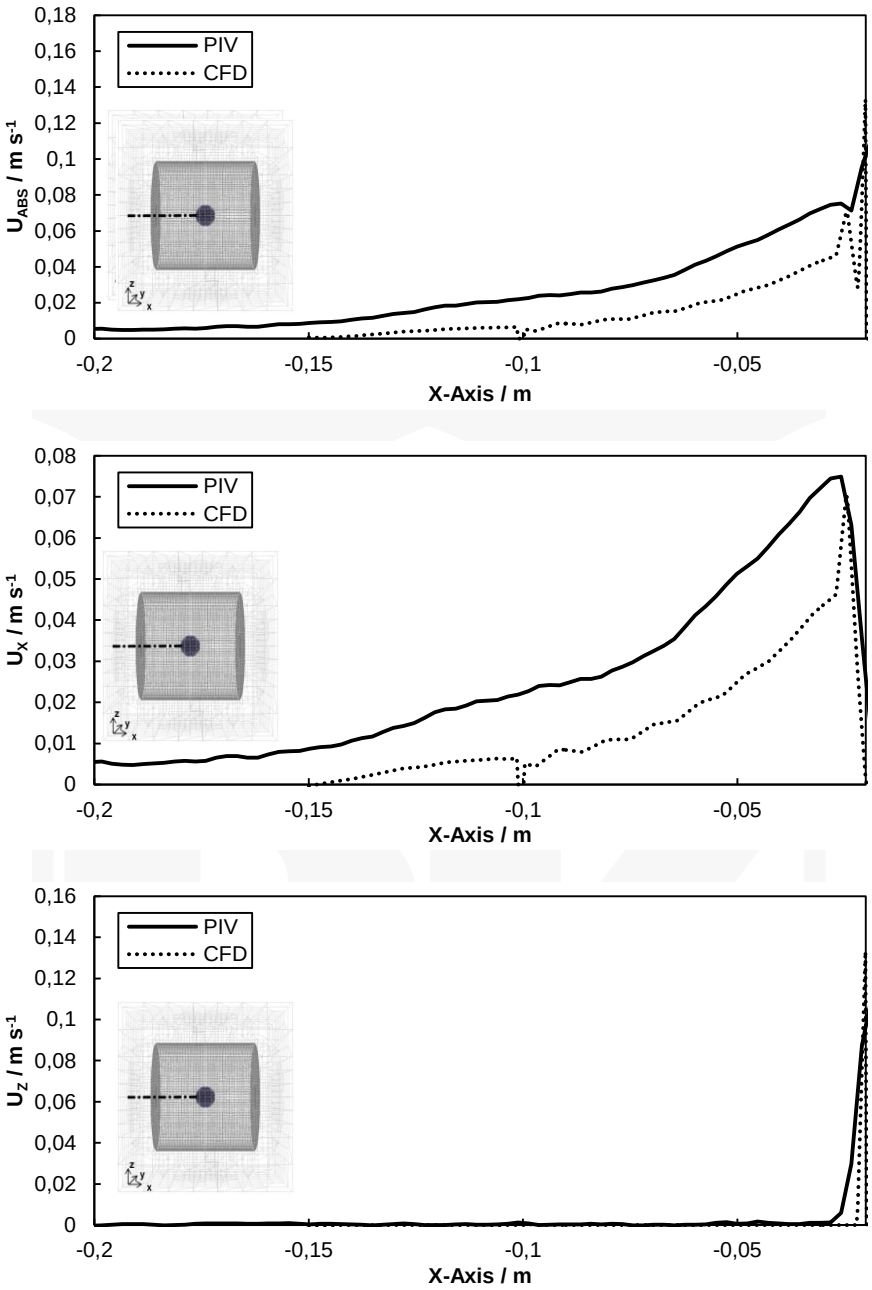

Fig. 5. Velocity profiles along the *x*-axis

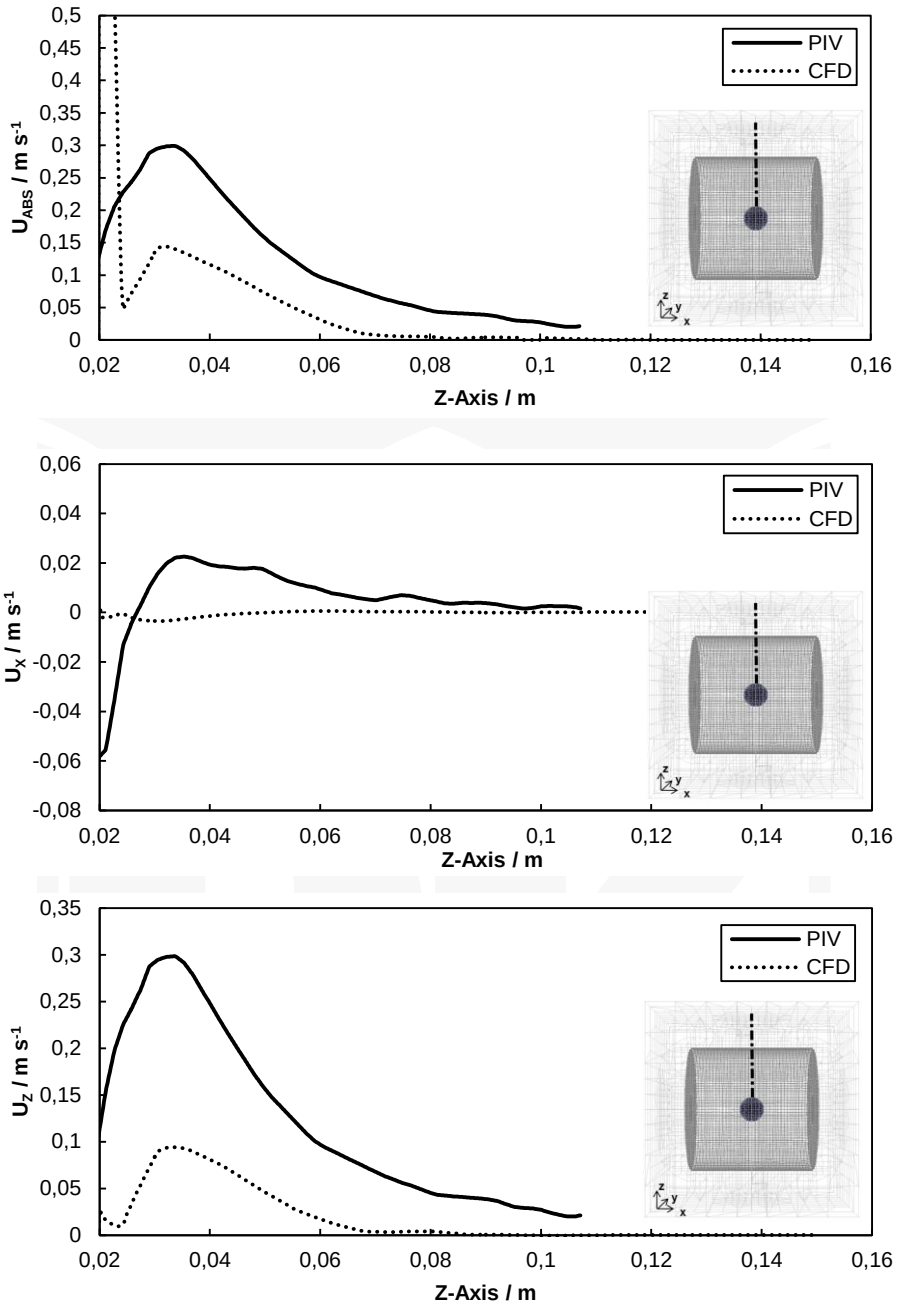

Fig. 6. Velocity profiles along the *z*-axis

Except for the x-component along the z-axis, the simulations fit well to the PIV measurements from a qualitatively perspective. The locations of the velocity maxima coincide, especially for the x-components in Figure 5 and the z-components in Figure 6. Also, general flow field characteristics like an inward flow at the poles and an outflow at the equator are predicted correctly. Quantitatively, the magnitude of all velocity components is underestimated. One explanation for this could be the relatively coarse mesh, which may not be sufficient to resolve the flow field accurately, especially in the vicinity of the sphere.

4. Conclusion

The OpenFOAM® tool used to calculate viscoelastic flows in rotating geometries presented in this work shows promising results. Compared to PIV measurements, the predicted flow field around a rotating sphere in a CMC solution simulated with a White-Metzner constitutive model fits qualitatively well; quantitatively, the velocity magnitudes were underestimated by a factor of roughly 3. In future works, simulations with finer meshes will be conducted to minimise numerical errors. Additionally, different differential constitutive models – especially multi-mode variants like Giesekus and Phan-Thien-Tanner – will be tested for improvement of simulation accuracy. Both PIV measurements and CFD simulations will also be conducted for more complex stirrer geometries like Rushton turbines and propellers.

References

[1] Weissenberg K., *Abhandlungen der Königlichen Preußischen Akademie der Wissenschaften zu Berlin Nr. 2*, 1931.

[2] Ide Y., White J.L., *Rheological phenomena in polymerization reactors: Rheological properties and flow patterns around agitators in polystyrene–styrene solutions*, Journal of Applied Polymer Science, vol. 18(10), 1974, 2997-3018.

[3] Garuno I.E., Tamaddon-Jahromi H.R., Webster M.F., *Oldroyd-B numerical solutions about a rotating sphere at low Reynolds number*, Rheologica Acta, vol. 54(3), 2015, 235-251.

[4] Cherizol R., Sain M., Tjong J., *Review of Non-Newtonian Mathematical Models for Rheological Characteristics of Viscoelastic Composites*, Green and Sustainable Chemistry, vol. 5(1), 2015, 6-14.

[5] White J.L., Metzner A.B., *Development of constitutive equations for polymeric melts and solutions*, Journal of Applied Polymer Science, vol. 7, 1963, 1867-1889.

[6] Favero J.L., Secchi A.R., Cardozo N.S.M, Jasak H., *Viscoelastic flow analysis using the software OpenFOAM and differential constitutive equations*, Journal of Non-Newtonian Fluid Mechanics, vol. 165, 2010, 1625-1636.

[7] Jasak H., *Dynamic Mesh Handling in OpenFOAM*, 47th AIAA Aerospace Sciences Meeting Including The New Horizons Forum and Aerospace Exposition, Orlando, Florida, 2009, 1-10.

[8] Versteeg H., Malalasekera W., *An Introduction to Computational Fluid Dynamics: The Finite Volume Method*, Pearson Education Limited 2007.

[9] Issa R.I., *Solution of implicitly discretized fluid flow equations by operator-splitting*, Journal of Computational Physics, vol. 93(2), 1991, 388-410.